

Journal of Materials Chemistry C

Accepted Manuscript



This is an *Accepted Manuscript*, which has been through the Royal Society of Chemistry peer review process and has been accepted for publication.

Accepted Manuscripts are published online shortly after acceptance, before technical editing, formatting and proof reading. Using this free service, authors can make their results available to the community, in citable form, before we publish the edited article. We will replace this *Accepted Manuscript* with the edited and formatted *Advance Article* as soon as it is available.

You can find more information about *Accepted Manuscripts* in the [Information for Authors](#).

Please note that technical editing may introduce minor changes to the text and/or graphics, which may alter content. The journal's standard [Terms & Conditions](#) and the [Ethical guidelines](#) still apply. In no event shall the Royal Society of Chemistry be held responsible for any errors or omissions in this *Accepted Manuscript* or any consequences arising from the use of any information it contains.



Journal Name

ARTICLE

Spatially inhomogeneous, stepwise phase transitions in a thiazyl diradical: A structural mismatch induced by lattice transformation

Rie Suizu,^{a,d} Akito Iwasaki,^b Yoshiaki Shuku,^b and Kunio Awaga^{c,d}Received 00th January 20xx,
Accepted 00th January 20xx

DOI: 10.1039/x0xx00000x

www.rsc.org/

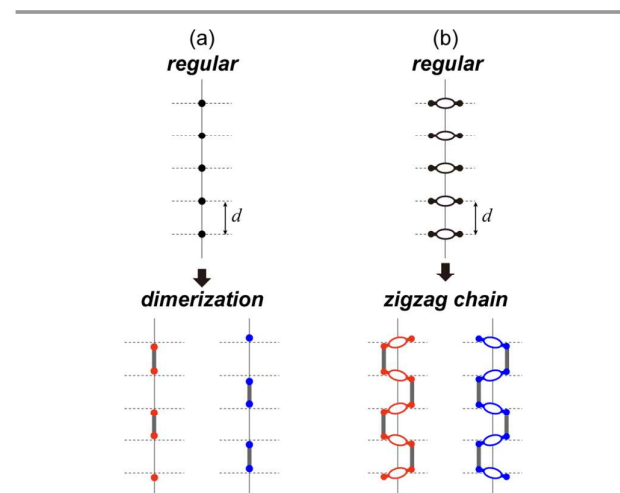
A heterocyclic thiazyl diradical, bis(1,2,3,5-dithiadiazolyl)-4,4'-biphenylene (**1**), was synthesized, and its structural and thermodynamic properties were characterized. This compound exhibits unique spatially inhomogeneous, first-order phase transitions at 306 and 359 K, in a stepwise fashion. The unit cell in the high-temperature phase above 359 K consists of four regular π -stacking columns with the same stacking manners having a uniform interplanar distance d . These four columns are connected by intermolecular S \cdots S and S \cdots N contacts between the thiazyl radical moieties, but the molecular planes are shifted by a distance of $d/4$ due to a steric hindrance between the bulky biphenylene moieties. Below 359 K, three of the four stacking columns exhibit structural transitions toward zigzag chain structures, formed by an alternating dimerization between the radical moieties, while one column maintains the uniform π stacking. In the low-temperature phase below 306 K, the last column finally exhibits the radical dimerization toward a zigzag chain structure. These unique phase transitions in **1** can be understood in terms of the stepwise transitions from “dimer liquid” to “dimer solid” through “dimer soliton phase”.

Introduction

The solid-state properties of organic radicals have been investigated for more than five decades, and various unique electrical and magnetic properties have been revealed so far.¹ These materials often exhibit a characteristic structural phase transition between a uniform structure at high temperatures and a dimerized structure at low temperatures reflecting their strong electron-lattice and/or spin-lattice interactions with a drastic jump in the temperature dependence of the magnetic susceptibility (Scheme 1).^{2–6} These transitions have been believed to be caused by the instability of the 1D antiferromagnetic chain of $S=1/2$, namely, spin-Peierls instability,⁷ but have been found even in 3D network structures of organic radicals. For instance, heterocyclic thiazyl radicals usually form the multi-dimensional crystal structures caused by face-to-face π overlaps and side-by-side S \cdots S and S \cdots N contacts.^{2,3,5,8,9} An $S=1/2$ radical, TTTA (=1,3,5-trithia-2,4,6-triazapentalenyl), exhibits a first-order phase transition between a dimerized low-temperature phase and a regular high-temperature phase with a surprisingly wide thermal hysteresis loop of *ca.* 100 K around room temperature.² It was recently proposed that thermal fluctuation in a

double-well potential of two dimerized structures can induce a phase transition toward a uniform structure upon heating, in which the entropy term plays a significant role.^{2d}

In the present work, we synthesized a diradical, bis(1,2,3,5-dithiadiazolyl)-4,4'-biphenylene (**1**, see Scheme 2), in which the molecular structure consists of a bulky biphenylene moiety and two terminal 1,2,3,5-dithiadiazolyl radical moieties. The structural and thermodynamic characterizations revealed unique phase transitions, which is caused by “bond frustration” and correspond to the stepwise transitions from “dimer liquid” to “dimer solid” through “dimer soliton phase”.



Scheme 1. The dimerization patterns. (a) monoradical, (b) diradical with a central bulky group and two terminal radical moieties.

^a Department of Nanomaterials Science, Graduate School of Advanced Integration Science, Chiba University, 1-33 Yayoi-cho, Inage-ku, Chiba 263-8522, Japan.

^b Department of Chemistry, Graduate School of Science, Nagoya University, Furo-cho, Chikusa-ku, Nagoya 464-8602, Japan.

^c Research Center for Materials Science, Nagoya University, Furo-cho, Chikusa-ku, Nagoya 464-8602, Japan.

^d JST-CREST, Nagoya University, Furo-cho, Chikusa-ku, Nagoya 464-8602, Japan

†Electronic Supplementary Information (ESI) available: The additional structural parameters of the single crystal structure analyses and the additional magnetic data are included. See DOI: 10.1039/x0xx00000x

Results and discussion

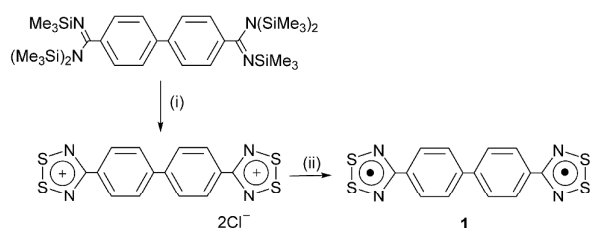
Synthesis and DSC measurements

The synthetic methodology for generating bifunctional dithiadiazolyls has been well established.⁹ We prepared **1**, following the procedure shown in Scheme 2. Namely, the reaction of the amidine compound with SCl_2 gave the crude dication compound, which was reduced to **1** with SbPh_3 . The crude compound of **1** was purified by fractional sublimations, affording black reflective needles. The total yield of the steps (i) and (ii) in Scheme 2 was 47%. The crystals of **1** were stable enough to be handled in air for at least several hours, as were the other bifunctional dithiadiazolyls.⁹

The DSC measurements for **1** were performed in the temperature range between 260 and 400 K. The results are shown in Figure 1. Upon heating from 280 K, an endothermic anomaly appears at 306 K (peak maximum), followed by a broad endothermic peak around 359 K (Fig. 1(a)). Upon cooling, the two transitions appear, making broad exothermic peaks at 359 and 306 K, suggesting that these transitions are not associated with hysteresis loops. The DSC curves clearly indicate the presence of two successive phase transitions. It is notable that the cooling curve exhibits broad tails on the low temperature sides of the two transitions (Figs. 1(b) and (c)). The transition enthalpies ΔH for the low- and high-temperature transitions are 52.3 and 179 J mol^{-1} , respectively. The latter is nearly three times larger than the former. It is concluded that material **1** exhibits three phases: a low-temperature (LT) phase below 306 K, a high-temperature (HT) phase above 359 K, and an intermediate-temperature (IT) phase between these temperatures.

Magnetic susceptibility

The temperature dependence of the molar magnetic susceptibility χ_M of **1** was examined in the range of 2–400 K under the field of 5000 Oe. The results are shown in the inset of Fig. 2, in which the values of χ_M exhibit significant increases below 50 K and above 250 K. The former is assignable to paramagnetic lattice defects. We calculated the intrinsic paramagnetic susceptibility χ_p , by subtracting the contribution of the Curie term at the low temperatures ($C = 1.78 \times 10^{-3} \text{ emu mol}^{-1}$) and the diamagnetic susceptibility ($-2.08 \times 10^{-4} \text{ emu mol}^{-1}$) from χ_M . Figure 2(a) shows the behavior of χ_p above 150 K, in which the two broken lines indicate the phase transition temperatures determined by DSC. While the χ_p plots make a change in gradient at 359 K, there is little anomaly at 306 K. Figure 2(b) shows the plots of $d\chi_p/dT$, which clearly indicate the anomalies at 306 and



Scheme 2. Reagents and conditions: (i) SCl_2 (excess), CH_3CN , 60 °C, 4 h, (ii) SbPh_3 (excess), CH_3CN , 60 °C, overnight, 47% yield.

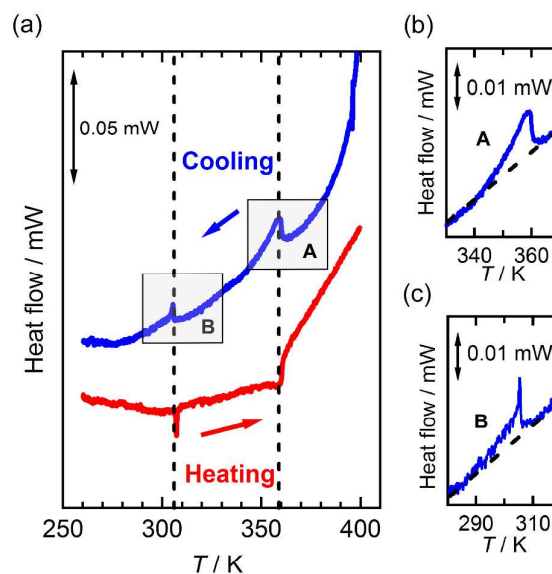


Figure 1. (a) The DSC curves for the diradical **1** upon heating (red curve) and cooling (blue curve) in the temperature range between 260 and 400 K. The panels (b) and (c) show the magnified figures around 359 and 306 K, respectively.

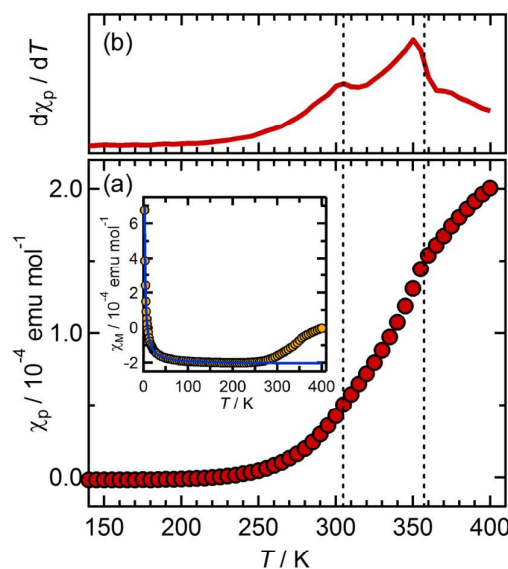


Figure 2. Temperature dependence of the paramagnetic susceptibility χ_p (a), and the differentiation, $d\chi_p/dT$ (b) (Inset: molar magnetic susceptibility, χ_M). The broken lines indicate the transition temperatures determined by DSC.

359 K. It is notable that χ_p exhibits no hysteresis loop in this temperature range, upon heating and cooling.

X-ray structural analysis for the HT phase

X-ray analyses of **1** were carried out at various temperatures in the range of 150–400 K. The crystallographic data are summarized in Tables 1. The crystal structure in the HT phase belongs to the orthorhombic space group $Fdd2$. The molecule **1**, in which a half of this unit is crystallographically asymmetric (Fig. 3(a)), is axially chiral due to the steric hindrance in the biphenyl

Table 1. Crystallographic data of **1**

Formula <i>M</i>	C ₁₄ H ₈ N ₄ S ₄ 360.48									
Temperature / K	150	200	250	280	300	320	340	360	380	400
Crystal system	Monoclinic							Orthorhombic		
Space group	P2 ₁ (#4)							Fdd2 (#43)		
<i>a</i> / Å	15.519(2)	15.537(2)	15.558(2)	15.563(3)	15.576(3)	15.588(3)	15.606(3)	15.611(4)	15.621(4)	15.629(4)
<i>b</i> / Å	7.0945(9)	7.1191(8)	7.1462(9)	7.1651(11)	7.1808(11)	7.1986(12)	7.219(2)	48.719(11)	48.764(11)	48.792(11)
<i>c</i> / Å	25.462(3)	25.488(4)	25.511(4)	25.523(4)	25.536(4)	25.549(5)	25.570(6)	3.6202(8)	3.6313(8)	3.6419(8)
α / °	90	90	90	90	90	90	90	90	90	90
β / °	107.6826(13)	107.686(2)	107.670(2)	107.672(2)	107.707(2)	107.737(2)	107.761(3)	90	90	90
γ / °	90	90	90	90	90	90	90	90	90	90
<i>V</i> / Å ³	2670.9(6)	2686.0(7)	2702.5(7)	2711.8(8)	2720.8(8)	2730.6(9)	2743.3(10)	2753.4(12)	2766.1(12)	2777.2(12)
<i>Z</i>	8	8	8	8	8	8	8	8	8	8
<i>D</i> _{calc} / g cm ⁻³	1.793	1.783	1.772	1.766	1.760	1.754	1.746	1.739	1.731	1.724
μ (Mo K α) / cm ⁻¹	7.104	7.064	7.020	6.996	6.973	6.948	6.916	6.891	6.859	6.832
<i>N</i> _{ref} (<i>R</i> _{int})	11699 (0.0230)	11756 (0.0237)	11844 (0.0261)	11893 (0.0256)	11935 (0.0253)	11913 (0.0239)	12017 (0.0268)	1524 (0.0234)	1528 (0.0211)	1529 (0.0217)
<i>R</i> ₁ [<i>I</i> > 2 σ (<i>I</i>)] ^a	0.0762	0.0747	0.0670	0.0604	0.0505	0.0417	0.0466	0.0304	0.0305	0.0319
<i>wR</i> ₂ ^b	0.2199	0.2038	0.1939	0.1716	0.1383	0.1179	0.1365	0.0783	0.0814	0.0837
Flack parameter	0.09(12)	0.11(12)	0.11(11)	0.11(9)	0.15(7)	0.04(6)	0.06(7)	0.01(11)	0.02(11)	0.09(11)
GOF ^c	1.120	1.119	1.093	1.102	1.066	1.046	1.069	1.103	1.108	1.083
CCDC	1017602	1017601	1017600	1017599	1017598	1017597	1017596	1017595	1017594	1017593

^a $R_1 = \sum ||F_o| - |F_c|| / \sum |F_o|$. ^b $wR_2 = [\sum \{w(F_o^2 - F_c^2)^2\} / \sum w(F_o^2)^2]^{1/2}$. ^c GOF = $[\sum \{w(F_o^2 - F_c^2)^2\} / (N_o - N_v)]^{1/2}$

rings, and the HT phase is racemic, consisting of the (+) and (−) enantiomers, which include the clockwise and counterclockwise rotations of the phenyl ring, respectively, along the molecular long axis (Fig. 3(b)). The torsion angle between the dithiadiazolyl and phenyl rings (N1-C1-C2-C3) is $-16.3(4)^\circ$. All the internal bond lengths and angles are typical of those seen in the other bifunctional dithiadiazolyls.⁹ The C_{dithiazolyl}-C_{phenylene} (C1-C2) and C_{phenylene}-C_{phenylene} (C7-C7') bond lengths indicate that the biphenylene moiety is in the aromatic form rather than the quinoid form; **1** should be regarded as a disjoint diradical. As found in the structures of the related bifunctional dithiadiazolyls,⁹ the molecular structure of **1** is bowed (Fig. 3(c)). This

bowed structure maximizes the intermolecular overlaps through the S \cdots S and S \cdots N contacts in both the π -stacking and lateral directions, and reduces the biphenylene-biphenylene repulsions in the former direction.

The crystal structure in the HT phase consists of a regular π -stacking column along the *c* axis and intercolumnar side-by-side interactions between the dithiadiazolyl rings. Figure 4(a) shows a side view of the π stacking in the HT phase at 400 K, which is formed by a π - π face-to-face overlap between the dithiadiazolyl rings with a constant interplanar distance *d* of 3.6419(8) Å. Figure 5(a) depicts a projection of the unit cell along the *c* axis, showing a network of the stacking columns. The columns denoted by **A**, **B**, **C** and **D** in this figure consist of the (+), (−), (+) and (−)-enantiomers, respectively. The π stacking manners in the four are the same, but the molecular planes in them are shifted by *d*/4 along the *c* axis. The network is formed by the side-by-side contacts between the dithiadiazolyl rings in the order of $\cdots\mathbf{A}\cdots\mathbf{B}\cdots\mathbf{C}\cdots\mathbf{D}\cdots\mathbf{A}\cdots\mathbf{B}\cdots\mathbf{C}\cdots\mathbf{D}\cdots$ along the *a* and *b* axes, as indicated by the green and red zigzag lines, respectively, in Fig. 5(a). This means that **A** or **C** forms S \cdots S and S \cdots N contacts with **B** and **D**, but there is a steric repulsion between the biphenyl rings of **A** and **C**, despite the fact that **A** and **C** neighbor each other along the *a* axis. This feature is the same for **B** or **D** with respect to **A** and **C**. This structure can be understood as follows. Due to steric effects between the biphenylene rings, the molecular planes of **A** and **C** are shifted by a distance of *d*/2 along the *c* axis. To make side-by-side short contacts between the radical moieties, the molecular planes of **B** and **D** are located at the midpoint between **A** and **C**, namely at *d*/4 and *3d*/4. It is characteristic of the HT phase to include

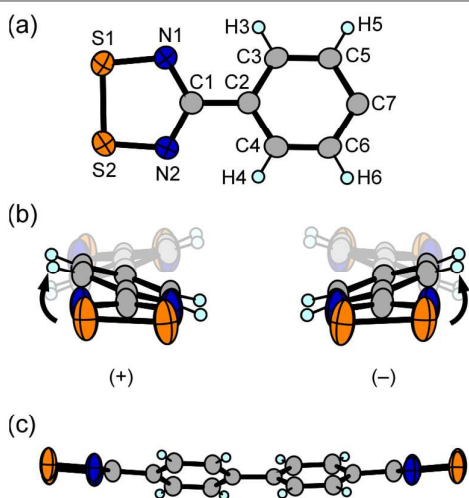


Figure 3. The molecular structures of **1** at 400 K; (a) asymmetry unit, (b) (+) and (−) enantiomers, and (c) side view along the molecular short axis.

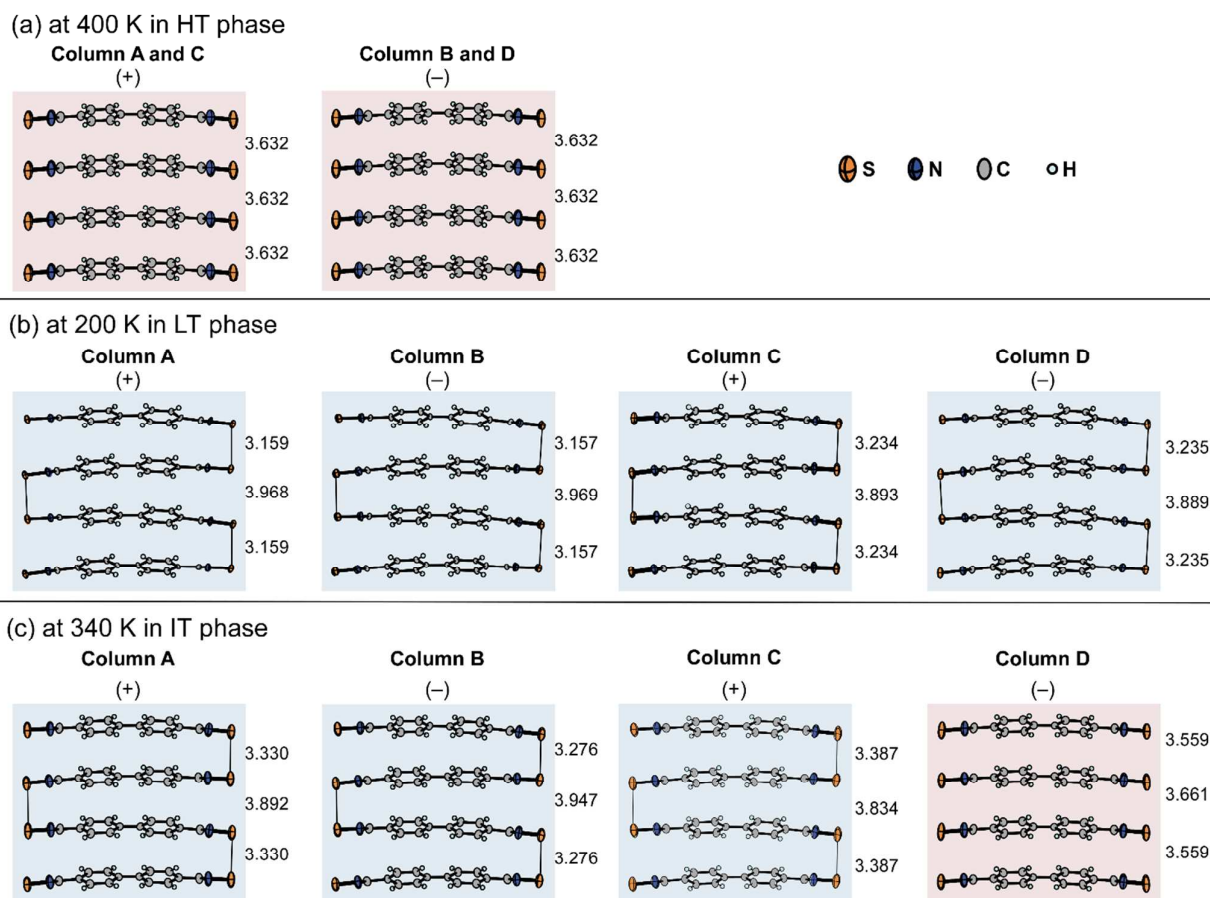


Figure 4. π Stacking modes in the three phases of **1**; (a) at 400 K in the HT phase, (b) 200 K in the LT phase, and (c) 340 K in the IT phase.

the stair-like arrays of the molecular planes of **1** with a step height of $d/4$ (see Fig. 8).

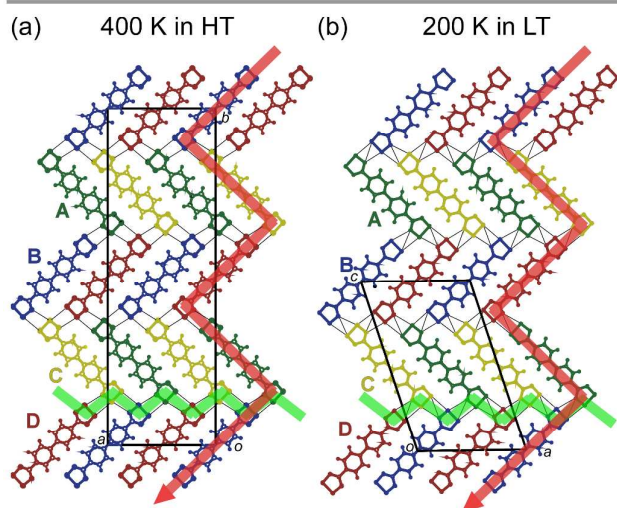


Figure 5. Projections of the unit cells at 400 (a) and 200 K (b), along the π -stacking directions.

X-ray structural analysis for IT and LT phases

The temperature dependence of the X-ray ω oscillation diffraction images was examined in the temperature range of 150–400 K. The results are shown in Fig. 6, and clearly indicate a lattice dimerization below 340 K. Wispy streaks are seen at $c^*/2$ at 400 K (see Figure 6(a)) due to a thermal fluctuation toward dimerization, while the structural analysis indicated the non-dimerized structure for the HT phase. Therefore, the HT phase should be regarded as a “dimer liquid”. The intensities of the wispy streaks gradually increase upon cooling, and, below 340 K, the Bragg’s peaks appear at $c^*/2$ accompanied with the wispy streaks, indicating a long-range lattice dimerization along the l direction (c axis) in the orthorhombic cell. A further cooling to below 300 K completely turns these weak streaks into Bragg’s peaks. The crystal structures of the IT and LT phases belong to the same space group, $P2_1$. The unit cell consists of four crystallographically independent molecules **A**–**D**, which can be corresponded to the molecules **A**–**D** in the HT phase, respectively.

In the crystal structure of the IT or LT phase, each of **A**–**D** separately forms a π stacking column with the 2_1 screw axes along the monoclinic b axis. Figure 5(b) shows a projection of the unit cell for the LT phase along the b axis, which is very

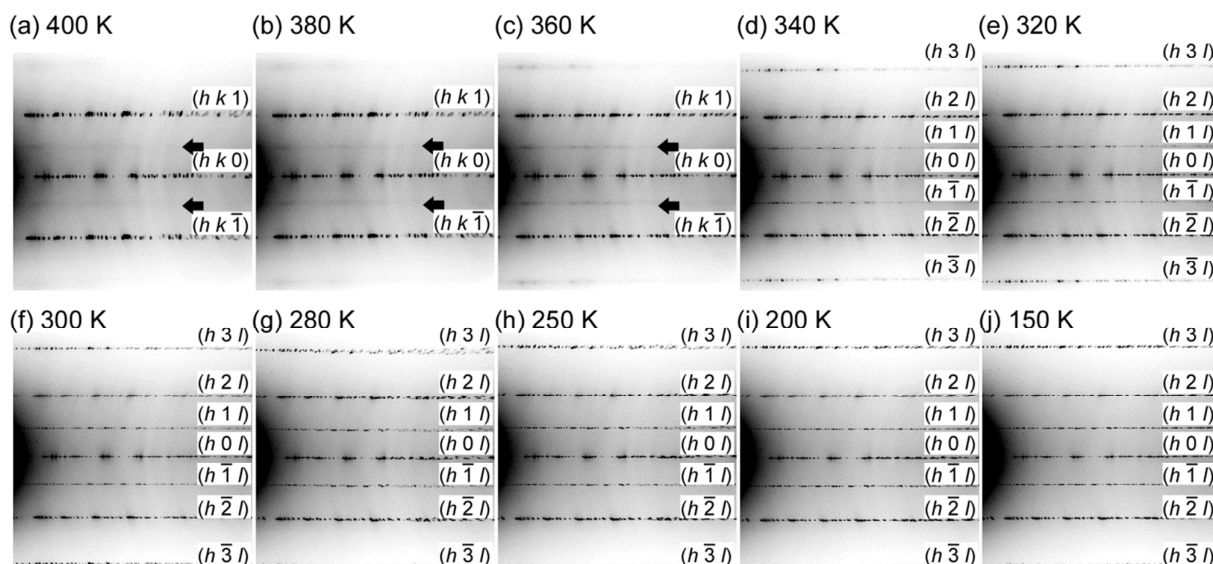


Figure 6. X-ray ω -oscillation diffraction images of **1** at various temperatures in the range of 400–150 K. (a) 400, (b) 380, (c) 360, (d) 340, (e) 320, (f) 300, (g) 280, (h) 250, (i) 200, and (j) 150 K.

similar to that for the HT phase in Fig. 5(a). However, the features of the π stackings in the IT and LT phases are significantly different from those of the HT phase. Figure 4(b) shows the π stackings at 200 K in the LT phase, which clearly exhibits an alternating dimerization—namely, a zigzag shape. Since there is no streak in this phase, the structure of the LT phase can be regarded as a “dimer solid”. The shorter intradimer distances and longer interdimer distances are ca. 3.2 and 3.9 Å, respectively. This was probably caused by the molecular structure of the diradical **1**, which consists of a central bulky group and two terminal radical moieties. Namely, the dimerization toward the zigzag chain would be more energetically preferable, to avoid the steric effects between the bulky central groups in the stacking chain.^{9f,9g} The structure of the LT phase is consistent with magnetic data, which indicate the presence of magnetic gap. As described later, the centroid positions for the molecules **A–D** exhibit significant shifts with respect to the stacking direction in the LT phase (See Figs. 8 and 10).

The crystal structure of the IT phase is unique, involving the coexistence of zigzag-chains and regular stacking structures. Figure 4(c) shows the π stackings at 340 K in this phase. The structure of **A–C** is nearly the same as that in the LT phase, exhibiting a zigzag-type dimerization. However, the structure of **D** at 340 K is significantly different from the other three; it is close to the regular stacking, which is similar to that in the HT phase. The coexistence of the regular and dimerized stackings can be characterized in terms of “dimer soliton phase”.

Structural features of the three phases

To confirm the successive, spatially inhomogeneous phase transitions in **1**, we analyzed the temperature dependence of the structural parameters. Figure 7 shows the temperature dependence of the intracolumnar, intermolecular $S\cdots S$ distances for the four stacking columns. These distances are defined in the

inset of this figure. At low temperatures below 250 K, namely in the LT phase, the $S\cdots S$ distances are clearly classified into two groups: the shorter ones (ca. 3.2 Å) and the longer ones (ca. 3.9 Å), reflecting the existence of the zigzag chains. The red plots in this figure indicate the $S\cdots S$ distances in the π stacking **D**; the intra- and inter-dimer $S\cdots S$ distances in this column gradually approach the same value of ca. 3.6 Å upon heating, in contrast to the weak temperature dependence of those in the other stackings. The zigzag chain in column **D** in the LT phase exhibits a gradual transformation to the regular stacking upon heating, even in the solid zigzag-chain structures of the neighboring columns **A–C**, and, in the IT phase between 306 and 359 K, column **D** can be effectively regarded as a regular stacking. In the HT phase, the crystal structure consists of the regular stacking of molecule **1**, so that the plots for the intra- and inter-dimer $S\cdots S$ distances merge into one above 359 K. Figure S1 shows the temperature dependence of the intercolumnar $S\cdots S$ distances. This figure also demonstrates the anomalous behav-

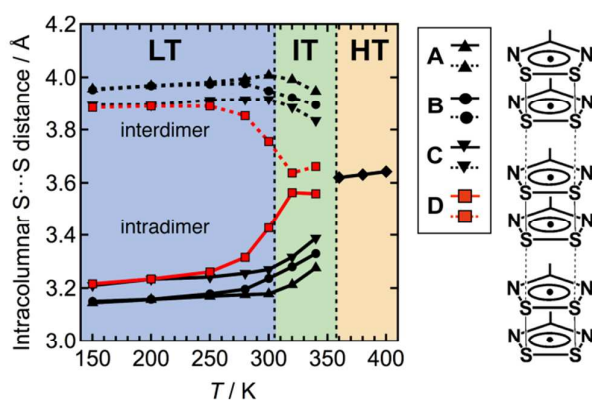


Figure 7. Temperature dependence of the intracolumnar, intermolecular $S\cdots S$ distances in the four stacking columns. The inset shows their definitions.

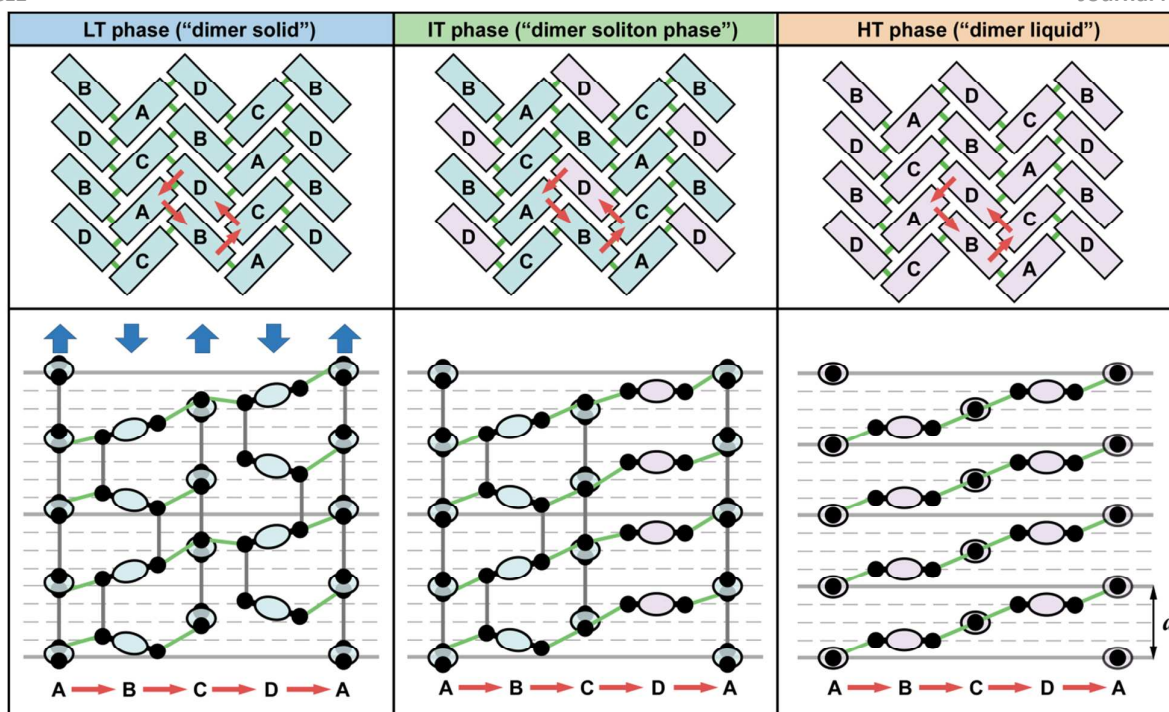


Figure 8. Top and side schematic views for the π stacking columns in the three phases of **1**.

ior of column **D**. These structural changes in **1** can be regarded as stepwise transitions from a regular to a zigzag-chain structure in which columns **A**–**C** exhibit the transition at 359 K and column **D** does so at 306 K. This agrees with the fact that the ratio of ΔH at the two transitions is almost 3:1.

The structural features of the three phases in **1** are schematically compared in Fig. 8, where the upper and lower panels show the top and side views of the π stacking columns, respectively. The lower panels show the unfold (developed view) figures of the four columns, which make a closed cycle, **A**–**B**–**C**–**D**–**A**, as indicated by the red arrows in the upper panels. This cycle is formed by the intercolumnar interactions among one side of the diradical molecules **A** and **C** and both sides of **B** and **D**. The thin gray and green lines indicate the intracolumnar zigzag dimerization, and the intercolumnar, intermolecular side-by-side short contacts between the radical moieties, respectively. The HT phase consists of the four regular stackings with an equivalent intermolecular distance d and the stair-like arrays of the molecular planes with a step height of $d/4$. While the IT phase includes three zigzag chain columns (**A**–**C**) and one regular column (**D**), all the stacking columns in the LT phase exhibit the zigzag dimerization. The blue bold arrows in the lower left panel indicate the shifts of the centroid positions for **A**–**D** in the LT phase (see Fig. 10). The structures of the four stacking columns **A**–**D** in the HT phase are not crystallographically independent; their π -stacking manners are the same and not distinguishable. Even so, three (**A**, **B** and **C**) of the four exhibit the structural transition, namely the dimerization toward the zigzag chain at 359 K, while the last one (**D**) exhibits the transition at 306 K. The diffraction images in Fig. 6 indicate that the HT, LT, and IT phases would correspond to “dimer liquid”, “dimer solid”, and “dimer soliton phase”, respectively. It is worth compar-

ing the features of column **D** and the so-called domain-wall that often appears in the phase transitions of low-dimensional molecular crystals.¹⁰ The structural features of column **D** in the IT phase are similar to those of a domain wall between the two dimerization (or zigzag) patterns. However, the concentration of the domain walls is usually very low and their locations are spatially random. It is thus unique that column **D** appears periodically in each unit cell (Fig. S2).

Mismatch induced by radical dimerization

We can now discuss the mechanism of the unique phase transitions. Figure 9 shows the transformations of the four stacking columns **A**–**D** from regular- to zigzag-chain structure. Figure 9(a-i) is identical to the lower panel for the HT phase in Fig. 8, namely a developed figure for the side views of the **A**–**D**, which makes a closed cycle with the intercolumnar interactions. Therefore, the **A** columns on the both sides are identical. In Fig. 9(a-ii), it is assumed that the zigzag-chain pattern propagates in the order **A**, **B**, **C**, **D**, making intercolumnar side-by-side overlaps between the radical moieties, as many as possible. In this case, the zigzag pattern of **A** is transferred to that of **B**, making many side-by-side contacts (green lines), and then the pattern **B** straightforwardly determines the structure of **C**. However, the zigzag pattern of **D** (red), which is transferred from **C**, can make less contact with the original chain **A**. It is obvious that there is another dimerization pattern for **D**, as shown in blue in Fig. 9(a-iii). The red and blue dimerization patterns are energetically equivalent, so that the phase transition from regular- to zigzag-chain structure should induce a “bond frustration”, which is caused by a mismatch among the zigzag dimerization patterns of the four stacking columns. This feature resembles to the frustration in gear trains (Fig. 9(b)); while, before gear rota-

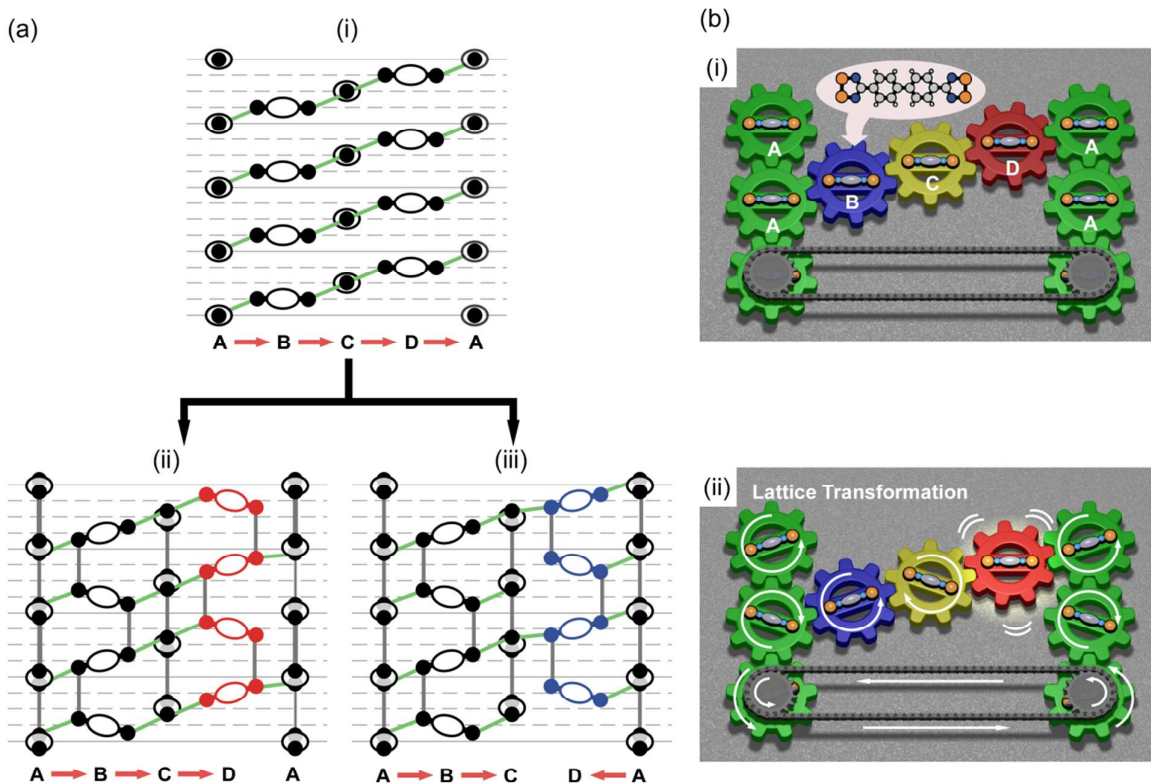


Figure 9. Bond frustration caused by a mismatch between the intracolumnar zigzag dimerizations and the intercolumnar interactions. (a-i) Schematic view for the crystal structure in the HT phase, which is identical to the lower right panel in Fig. 8. (a-ii and iii) Two possible structures expected after dimerization, in case that there is no shifts of the centroid positions. They are energetically equivalent, so that the intracolumnar dimerization would induce the intercolumnar bond frustration. (b) Frustrated gear train; while, before gear rotations, there is no obvious frustration (b-i), the rotations immediately induce frustration (b-ii).

tions, the frustration is not obvious, the rotations immediately induce frustration. Therefore, it is considered that this frustration would prevent the progress of the dimerization in column **D** and maintain the regular structure in the IT phase, even though the other three columns exhibit the dimerization.

We examined the crystal coordinates of the centroid positions for the molecules **A**–**D** in the three phases. Figure 10 shows the temperature dependence of the coordinate x along the π -stacking direction, namely the c axis for the HT phase or the b axis for the IT and LT phases. Since the unit-cell length along the stacking direction in the IT or LT phase is twice that in the HT phase due to the lattice dimerization, we plotted the $2x$ values for the IT and LT phases for the comparison with the data in the HT phase. In the HT phase, the x values for the centroid positions of **A**–**D** are close to 0, 0.25, 0.5 and 0.75, respectively, and even in the IT phase, where the three stacking columns exhibit the dimerization to the zigzag chains, these values depend little on temperature. This is understandable, because the regular π -stacking of the diradicals can make a transformation to a zigzag chain without changing the centroid position of each molecule (see Scheme 1(b)). Below 306 K in the LT phase, however, the coordinates of **B** and **D** decrease significantly, while those of **A** and **C** increase significantly. These shifts can be understood as follows. Since neither the red nor the blue dimerization pattern can maximize the intercolumnar contacts, as shown in Figs. 9(a-ii) and (a-iii), it is necessary to shift the centroid positions after the dimerization in column

D, in order to maximize the intercolumnar contacts and to relax the frustration. In other words, the remaining regular stacking structure of **D** in the IT phase is strong evidence for the bond frustration between two energetically equivalent dimerization patterns (red and blue). The significant shifts of the centroid positions in the LT phases are considered to reflect the frustration induced by the dimerization.

Conclusion

What we found in the present work is the presence of the three unique phases in **1**: “dimer liquid”, “dimer solid”, and “dimer soliton phase”. The unique structural phase transitions in **1** can be attributed to a mismatch between the intracolumnar zigzag dimerizations and the intercolumnar interactions, that is, “bond frustration”, which resembles to the frustration in gear trains. Geometrical frustration has been recognized as a result from an intrinsic incompatibility between certain fundamental interactions and the underlying lattice geometry. The most well-known example is the spin frustration for the antiferromagnetically interacting spins in a triangle,¹¹ and the complex ground states of the geometrically frustrated systems and the characteristic relaxation processes to the ground states have attracted much attention.¹¹ In contrast, the bond frustration in the present material was “induced” in the regular crystal structure with no obvious frustration. The induced frustration is considered to be universal in the organic radical crystals with strong electron-lattice and spin-lattice interactions, and is expected to open a

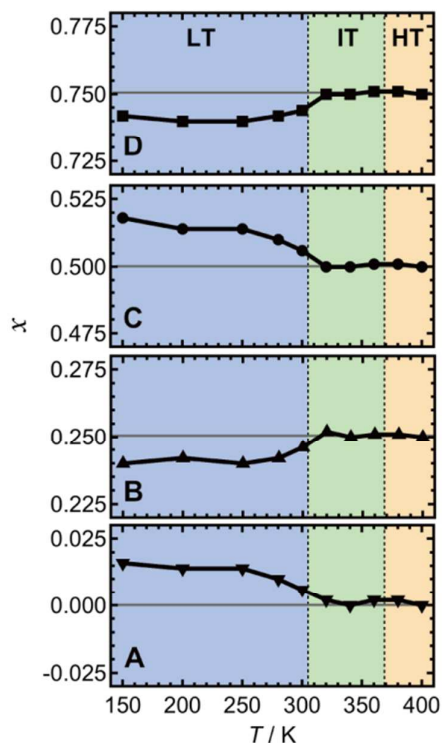


Figure 10. Temperature dependence of the centroid positions x for the molecules **A**, **B**, **C**, and **D** with respect to the c axis in the HT phase and the b axis in the IT and LT phases. The x values for the IT and LT phases are magnified by 2 for comparison with those for the HT phase, since the unit-cell length along the stacking direction in the IT or LT phase is twice that in the HT phase.

new branch in the chemistry and physics of geometrical frustration.

Experimental Section

General Remarks. All manipulations were carried out under a dry nitrogen atmosphere using Schlenk-tube techniques. 4,4'-Biphenylenebis[*N,N,N'*-tris(trimethylsilyl)carboxamidine] was prepared according to the literature procedures.¹² SbPh_3 , and anhydrous acetonitrile were used as received. Mass spectra were obtained on a JEOL JMS-700 instrument operating in electron impact (EI) mode. Elemental analysis was performed with a LECO CHNS-932 microanalyzer.

Synthesis of bis(1,2,3,5-dithiadiazolyl)-4,4'-biphenylene (1**).** An SbPh_3 (10 ml) was added dropwise from the dropping funnel into an acetonitrile (100 ml) suspension of 4,4'-biphenylenebis[*N,N,N'*-tris(trimethylsilyl)carboxamidine] (9.20 g, 13.6 mmol). The mixture was heated at 60 °C for 5 h and then filtered to afford a crude 4,4'-biphenylbis(1,2,3,5-dithiadiazolyl) dichloride as an orange powder. The crude dichloride salt was suspended to acetonitrile (100 ml) and large excess of SbPh_3 (12.0 g, 34.0 mmol) was added to it and heated at 60 °C for 5 h. After the reaction mixture was allowed to cool to room temperature, a black precipitate was filtered and purified by sublimation under reduced pressure (280 °C / 10^{-2} torr) to give **1** (2.31 g, 6.41 mmol, 47%) as a black needle. The char-

acterization was performed by MS, X-ray diffraction and elemental analyses. Mass (EI, 70 eV): m/z 360 (M^+ , 100), 314 ($\text{M}^+ - \text{S-N}$, 8), 282 ($\text{M}^+ - 2\text{S-N}$, 48), 236 ($\text{M}^+ - 3\text{S-2N}$, 19), 204 ($\text{M}^+ - 4\text{S-2N}$, 38). Anal. Found: C, 46.90; N, 15.30; H, 2.23. Calcd for $\text{C}_{14}\text{H}_8\text{N}_4\text{S}_4$: C, 46.64; N, 15.54; H, 2.24. The crystals of **1** were stable enough to be handled in air for at least several hours, as were the other bifunctional dithiadiazolyls.

DSC Measurement. The DSC measurements were performed on a Mettler Toledo DSC 822e/200 calorimeter with a scan rate of 1 K/min upon heating and cooling.

Single-crystal X-ray diffraction analyses. The X-ray diffraction data for single crystal structure analysis were collected on a Rigaku AFC-10 instrument equipped with a Saturn 70 CCD detector under a cold nitrogen stream, by using graphite-monochromated Mo $K\alpha$ radiation ($\lambda = 0.71070$ Å). Temperature was corrected with the thermocouple. The frame data were integrated and corrected for absorption with the Rigaku/MSC Crystal Clear package.¹³ The structures were solved by direct methods (SIR-97¹⁴) and standard difference map techniques, and were refined with full-matrix least-square procedures on F^2 . All calculations were performed using the Crystal Structure 4.0¹⁵ crystallographic software package except for refinement, which was performed using SHELXL-97.¹⁶ Anisotropic refinement was applied to all non-hydrogen atoms. All hydrogen atoms were placed at calculated positions and refined using a riding model.

We concluded the $P2_1$ space group for the structures below 340 K, though the ADDSYM in PLATON program¹⁷ suggested $Fdd2$ as an alternative. This space group means that the structure should consist of a regular-stacking column. However, the X-ray diffraction images in Figure 6 clearly indicate lattice dimerization below 340 K; Wispy streaks are seen at $c^*/2$ at 400 K (see Figure 6(a)) due to a thermal fluctuation toward dimerization. Below 340 K, the wispy streaks change into the Bragg's peaks, indicating a long-range lattice dimerization along the l direction (c axis) in the orthorhombic cell. Furthermore, we also found the diffractions, which were forbidden for the F -centered lattices, such as $h+k$, $k+l$, $l+h = 2n+1$ for (hkl) . The ADDSYM EXACT in PLATON did not find $Fdd2$. The checkCIF for the 150 K data alerted a large ADP max/min ratio of C44, and large residual electron densities. They are probably caused by a disorder between the two configurations for column **D**, resulting from the frustration. Crystal data for **1** have been deposited at the Cambridge Crystallographic Data Centre under the number CCDC-1017593 (400 K), 1017594 (380 K), 1017595 (360 K), 1017596 (340 K), 1017597 (320 K), 1017598 (300 K), 1017599 (280 K), 1017600 (250 K), 1017601 (200 K), 1017602 (150 K).

Magnetic Susceptibility. Magnetic measurements were carried out on a SQUID (Quantum Design MPMS XL) magnetometer under 5000 Oe in the temperature range of 2-400 K.

Acknowledgements

This work was supported by a Grant-in-Aid for Scientific Research from the Ministry of Education, Culture, Sports, Science, and Technology (MEXT). Funds were also provided by

the JSPS Core-to-Core Program, A. Advanced Research Networks.

Notes and references

- 1 R. G. Hicks, *Org. Biomol. Chem.*, 2007, **5**, 1321.
- 2 (a) W. Fujita and K. Awaga, *Science*, 1999, **286**, 261. (b) G. D. McManus, J. M. Rawson, N. Feeder, J. van Duijn, E. J. L. McInnes, J. J. Novoa, R. Burriel, F. Palacio, and P. Oliete, *J. Mater. Chem.*, 2001, **11**, 1992. (c) W. Fujita, K. Awaga, H. Matsuzaki, and H. Okamoto, *Phys. Rev. B*, 2002, **65**, 064434. (d) S. Vela, F. Mota, M. Deumal, R. Suizu, Y. Shuku, A. Mizuno, K. Awaga, M. Shiga, J. J. Novoa, and J. Riba-Arino, *Nat. Commun.*, 2014, **5**, 4411.
- 3 (a) T. M. Barkley, A. W. Cordes, N. A. George, R. C. Haddon, M. E. Itkis, M. S. Mashuta, R. T. Oakley, G. W. Patenaude, R. W. Reed, J. F. Richardson, and H. Zhang, *J. Am. Chem. Soc.*, 1998, **120**, 352. (b) J. L. Brusso, O. P. Clements, R. C. Haddon, M. E. Itkis, A. A. Leitch, R. T. Oakley, R. W. Reed, and J. F. Richardson, *J. Am. Chem. Soc.*, 2004, **126**, 8256. (c) J. L. Brusso, O. P. Clements, R. C. Haddon, M. E. Itkis, A. A. Leitch, R. T. Oakley, R. W. Reed, and J. F. Richardson, *J. Am. Chem. Soc.*, 2004, **126**, 14692. (d) A. Alberola, R. J. Collis, S. M. Humphrey, R. J. Less, and J. M. Rawson, *Inorg. Chem.*, 2006, **45**, 1903. (e) A. Alberola, D. J. Eisler, L. Harvey, and J. M. Rawson, *CrystEngComm*, 2011, **13**, 1794.
- 4 M. E. Itkis, X. Chi, A. W. Cordes, and R. C. Haddon, *Science*, 2002, **296**, 1443.
- 5 (a) C. M. Robertson, A. A. Leltch, K. Cvrkalj, R. W. Reed, D. J. T. Myles, P. A. Dube, and R. T. Oakley, *J. Am. Chem. Soc.*, 2008, **130**, 8414. (b) K. Lakin, S. M. Winter, L. E. Downie, X. Bao, J. S. Tse, S. Desgreniers, R. A. Secco, P. A. Dube, and R. T. Oakley, *J. Am. Chem. Soc.*, 2010, **132**, 16212.
- 6 Fatila, E. M.; Mayo, R. A.; Rouzières, M.; Jennings, M. C.; Dechambenoit, P.; Soldatov, D. V.; Mathonière, C.; Clérac, R.; Coulon, C.; Preuss, K. E. *Chem. Mater.*, 2015, **27**, 4023.
- 7 J. W. Bray, H. R. Hart, Jr., L. V. Interrante, L. S. Jacobs, J. S. Kasper, G. D. Watkins, S. H. Wee, and J. C. Bonner, *Phys. Rev. Lett.*, 1975, **35**, 744.
- 8 (a) J. M. Rawson, A. Alberola, and A. Whalley, *J. Mater. Chem.*, 2006, **16**, 2560. (b) K. Awaga, T. Tanaka, T. Shirai, M. Fujimori, Y. Suzuki, H. Yoshikawa, and W. Fujita, *Bull. Chem. Soc. Jpn.*, 2006, **79**, 25. (c) K. Awaga, K. Nomura, H. Kishida, W. Fujita, H. Yoshikawa, M. M. Matsushita, L. Hu, Y. Shuku, and R. Suizu, *Bull. Chem. Soc. Jpn.*, 2014, **87**, 234.
- 9 (a) A. W. Cordes, R. C. Haddon, R. T. Oakley, L. F. Schneemeyer, J. V. Waszczak, K. M. Young, and N. M. Zimmerman, *J. Am. Chem. Soc.*, 1991, **113**, 582. (b) A. W. Cordes, C. M. Chamchoumis, R. G. Hicks, R. T. Oakley, K. M. Young, and R. C. Haddon, *Can. J. Chem.*, 1992, **70**, 919. (c) A. W. Cordes, R. C. Haddon, C. D. MacKinnon, R. T. Oakley, G. W. Patenaude, R. W. Reed, T. Rietveld, and K. E. Vajda, *Inorg. Chem.*, 1996, **35**, 7626. (d) C. D. Bryan, A. W. Cordes, R. C. Haddon, R. G. Hicks, R. T. Oakley, T. T. M. Palstra, and A. J. Perel, *J. Chem. Soc., Chem. Commun.*, 1994, 1447. (e) C. D. Bryan, A. W. Cordes, J. D. Goddard, R. C. Haddon, R. G. Hicks, C. D. MacKinnon, R. C. Mawhinney, R. T. Oakley, T. T. M. Palstra, and A. S. Perel, *J. Am. Chem. Soc.*, 1996, **118**, 330. (f) M. P. Andrews, A. W. Cordes, D. C. Douglass, R. M. Fleming, S. H. Glarum, R. C. Haddon, P. Marsh, R. T. Oakley, T. T. M. Palstra, L. F. Schneemeyer, G. W. Trucks, R. Tycko, J. V. Waszczak, K. M. Young, and N. M. Zimmerman, *J. Am. Chem. Soc.*, 1991, **113**, 3559. (g) A. W. Cordes, R. C. Haddon, R. G. Hicks, D. K. Kennepohl, R. T. Oakley, T. T. M. Palstra, L. F. Schneemeyer, S. R. Scott, and J. V. Waszczak, *Chem. Mater.*, 1993, **5**, 820. (h) R. A. Beekman, R. T. Boéré, K. H. Moock, and M. Parvez, *Can. J. Chem.*, 1998, **76**, 85. (i) T. M. Barclay, A. W. Cordes, N. A. George, R. C. Haddon, M. E. Itkis, and R. T. Oakley, *Chem. Commun.*, 1999, 2269.
- 10 H. Kishida, H. Takamatsu, K. Fujinuma, and H. Okamoto, *Phys. Rev. B*, 2009, **80**, 205201.
- 11 L. Balents, *Nature*, 2010, **464**, 199.
- 12 R. Gompper, H.-J. Mair, and K. Polborn, *Synthesis*, 1997, 696.
- 13 CrystalClear: Rigaku Corporation, 1999. CrystalClear Software User's Guide, Molecular Structure Corporation, 2000. J. W. Pflugrath *Acta Cryst.*, 1999, **D55**, 1718.
- 14 A. Altomare, M. Burla, M. Camalli, G. Cascarano, C. Giacovazzo, A. Guagliardi, A. Moliterni, G. Polidori, and R. Spagna, *J. Appl. Cryst.*, 1999, **32**, 115.
- 15 CrystalStructure 4.0: Crystal Structure Analysis Package, Rigaku Corporation (2000-2010). Tokyo 196-8666, Japan.
- 16 G. M. Sheldrick, *Acta Cryst.*, 2008, **A64**, 112.
- 17 PLATON: A. L. Spek, *Acta. Cryst.*, 2009, **D65**, 148.

*Table of Contents entry***Spatially Inhomogeneous, Stepwise Phase Transitions in a Thiazyl Diradical:
A Structural Mismatch Induced by Lattice Transformation**

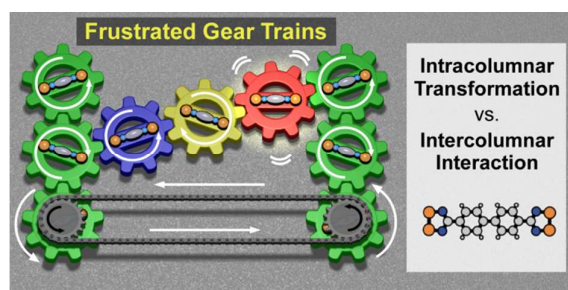
Rie Suizu,^{*,†,‡} Akito Iwasaki,[§] Yoshiaki Shuku,[§] Kunio Awaga^{*,‡,#}

[†]Department of Nanomaterials Science, Graduate School of Advanced Integration Science, Chiba University, 1-33 Yayoi-cho, Inage-ku, Chiba 263-8522, Japan

[‡]JST-CREST, Nagoya University, Furo-cho, Chikusa-ku, Nagoya 464-8602, Japan

[§]Department of Chemistry, Graduate School of Science, Nagoya University, Furo-cho, Chikusa-ku, Nagoya 464-8602, Japan

[#]Research Center for Materials Science, Nagoya University, Furo-cho, Chikusa-ku, Nagoya 464-8602, Japan



A heterocyclic thiazyl diradical, bis(1,2,3,5-dithiadiazolyl)-4,4'-biphenylene, exhibits spatially inhomogeneous, stepwise phase transitions at 306 and 359 K, which are caused by a “bond frustration“, induced by a mismatch between the intracolumnar transformations and the intercolumnar interactions, as happens in frustrated gear trains.